

ARTICLE



High-fat diet-induced nonalcoholic steatohepatitis is accelerated by low carnitine and impaired glucose tolerance in novel murine models

Yui Terayama¹, Shin-ichi Nakamura^{1,2}, Kazuyuki Mekada³, Tetsuro Matsuura¹ and Kiyokazu Ozaki¹

© The Author(s), under exclusive licence to United States and Canadian Academy of Pathology 2022

Carnitine deficiency and impaired glucose tolerance (IGT) exacerbate liver steatosis. Given the current lack of ideal murine nonalcoholic steatohepatitis (NASH) models, we investigated new NASH models using *jvs/+* mice with low carnitine and wild-type mice with low-dose alloxan-induced IGT. The *jvs/+* and wild-type mice were divided into *jvs/+* mice fed a high-fat diet (HFD) from 3 weeks of age (HF hetero group), wild-type mice with low-dose alloxan treatment fed HFD (AL + HF wild group), wild-type mice fed HFD (HF wild group), and two types of mice fed a normal diet—*jvs/+* and wild-type (intact group). All mice were sacrificed at 20 or 40 weeks of age. All male HFD-fed mice showed obesity, IGT, high blood insulin levels, homeostatic model assessment of insulin resistance (HOMA-IR), high liver enzyme levels, and high cholesterol levels. The degree of IGT was the worst in the AL + HF wild group, and blood insulin levels and HOMA-IR score were remarkably increased from 20 to 40 weeks of age. Almost all HFD-fed mice showed steatosis, fibrosis, and lobular inflammation in the centrilobular zone. These changes were accompanied by hepatocyte ballooning and were enhanced at 40 weeks of age. Furthermore, the incidence rate of nodular hyperplasia and adenoma in both the HF hetero and AL + HF wild groups was nearly 30%. We successfully established two novel murine models of NASH using male *jvs/+* mice with low carnitine and male wild-type mice with IGT that eventually developed obesity, fatty liver, insulin resistance, liver fibrosis, and tumorigenesis. These results suggest that low carnitine levels and early-stage induction of IGT are important factors in the progression of NASH to tumorigenesis, similar to human NASH.

Laboratory Investigation (2022) 102:621–630; <https://doi.org/10.1038/s41374-022-00732-8>

INTRODUCTION

Nonalcoholic fatty liver disease (NAFLD) is characterized by the development of fatty liver in the absence of alcohol abuse. Recently, it has attracted attention as the most common liver disease that leads to metabolic syndromes^{1–3}. NAFLD comprises two disease mechanisms: simple intrahepatic fat accumulation and nonalcoholic steatohepatitis (NASH). NASH is a nutritionally impaired chronic progressive liver disease—similar to alcoholic hepatitis—that progresses to fatty liver, hepatitis, liver fibrosis, liver cirrhosis, and eventually to a liver tumor. Two pathogenesis mechanisms have been proposed. First, the two-hit theory, wherein a first “hit”, such as obesity, hyperlipidemia, impaired glucose tolerance (IGT), diabetes, high insulin levels, and insulin resistance (IR) due to metabolic syndrome, causes hepatic steatosis, and the occurrence of a second “hit”, such as inflammatory cytokine release and oxidative stress, causes steatohepatitis⁴.

The second proposed mechanism is the multiple parallel hit theory, which hypothesizes that environmental, metabolic, and genetic factors contribute to the development and progression of complicated NASH⁵.

Many NASH animal models have been proposed; however, there is no suitable model for the development of obesity, fatty

liver, insulin resistance, fibrosis, and tumors similar to human disease^{6,7}. Diet-induced NASH models using a high-fat diet (HFD) develop obesity, insulin resistance, and IGT, but they do not show marked steatohepatitis, and the incidence of tumors is low^{6–8}. Stelic animal model (STAM) mice treated with streptozotocin in addition to HFD develop hepatocellular carcinoma^{7,9}; however, this model is not associated with the development of obesity, with streptozotocin being a genotoxic carcinogen whose pathogenesis is different from human NASH. Therefore, it is necessary to establish a model that mimics human NASH's etiological and pathogenic nature.

The juvenile visceral steatosis (JVS) mouse is a mutant animal model for systemic carnitine deficiency caused by mutations in the *OCTN2* gene¹⁰. Homozygous *jvs/jvs* mice develop severe fatty liver and die at a young age because the lack of carnitine prevents the transport of long-chain fatty acids and accumulation of fat in various cells¹¹. Therefore, *jvs/jvs* mice cannot be used to study NASH due to premature death; however, heterozygous *jvs/+* mice have low carnitine levels, showing only a slight accumulation of lipids in hepatocytes, and can survive^{11–13}. Carnitine is reportedly related to one of the mechanisms behind NAFLD/NASH because carnitine treatment improves liver lesions in HFD-induced NASH

¹Laboratory of Pathology, Faculty of Pharmaceutical Science, Setsunan University, 45-1 Nagaotohge-cho, Hirakata, Osaka 573-0101, Japan. ²Kyoto Institute of Nutrition & Pathology Inc, 7-2 Furuiketani, Tachikawa, Ujita-cho, Tsuzuki-gun, Kyoto 610-0231, Japan. ³Department of Zoology, Okayama University of Science, 1-1 Ridai-cho, Kita-ku, Okayama City, Okayama 700-0005, Japan. email: ozaki@pharm.setsunan.ac.jp

Received: 4 June 2021 Revised: 29 December 2021 Accepted: 3 January 2022

Published online: 17 January 2022

model mice¹⁴. Thus, heterozygous *jvs/+* mice fed HFD may develop severe fatty liver progressing to a lesion similar to human NASH because of low carnitine levels.

IGT is a risk factor for NASH^{1–3}. Alloxan (AL) is a non-genotoxic drug that induces loss of insulin-producing islet β -cells and is commonly used to establish a type 1 diabetes animal model^{15,16}. Low-dose AL administration induces either transient hyperglycemia or IGT but restores hyperglycemia status by β -cell regeneration^{16,17}. Furthermore, very young mice have high resistance to the diabetogenic effect of AL, and IGT is transiently induced by AL treatment^{18,19}. Therefore, early-stage induction by AL treatment in neonatal mice may prolong the duration of IGT and deteriorate HFD-induced steatohepatitis in mice, similar to that in human NASH.

Drug sensitivity and disease susceptibility are mainly influenced by various factors, especially age and genetic background^{18–20}. Therefore, in this study, heterozygous *jvs/+* mice and wild-type *+/+* mice with the same genetic background were obtained and used for mating with heterozygous *jvs/+* mice, eliminating the genetic factors that influence the difference in susceptibility between all mice.

Herein, we attempted to establish a new HFD-induced NASH model similar to human NASH. We used heterozygous *jvs/+* mice with low carnitine and wild-type mice with neonatal AL-induced IGT based on the hypothesis that low carnitine levels or early-stage induction of IGT may further exacerbate hepatic steatosis induced by HFD feeding.

MATERIALS AND METHODS

Animals and housing condition

The homozygous *JVS (jvs/jvs)* mouse was originally identified as a mutant of the C3H strain²¹. The *jvs* gene was introduced into C57BL/6J mice using a backcross breeding system to obtain new strains of *JVS* mice. This *JVS* mutant line with a C57BL/6J genetic background was maintained by mating these mice with heterozygous *jvs/+* mice. Heterozygous *jvs/+* mice were further discriminated from wild-type *+/+* mice using microsatellite marker analysis²². In this study, heterozygous *jvs/+* and wild-type *+/+* mice with a C57BL/6J genetic background were obtained by breeding heterozygous *jvs/+* mice.

Heterozygous *jvs/+* or wild-type *+/+* mice were housed in TPX cages within a conventional environment, with a relative humidity of 40–70% and a temperature of 20–26 °C under a 12/12 h light/dark cycle. Ventilation was provided with filtered fresh air, and free access to tap water and food was allowed. Animal studies were performed in compliance with the ARRIVE guidelines. This study was approved by the Committee for Animal Experiments of Setsunan University (Approval number: K11-16, K12-18, K13-18, K14-19).

Experimental design

Sixty-eight heterozygous *jvs/+* and 137 wild-type *+/+* mice were divided into four groups: male heterozygous mice, female heterozygous mice, male wild-type mice, and female wild-type mice. Heterozygous mice were fed HFD (HFD-60, 60% kcal from fat; Oriental Yeast, Tokyo, Japan) from 3 weeks of age (HF hetero group). Wild-type mice were treated with AL (Sigma-Aldrich Japan, Tokyo, Japan) 3 days postpartum, followed by an HFD from 3 weeks of age (AL + HF wild group). As a positive control, wild-type mice were fed an HFD from 3 weeks of age (HF wild group). Additionally, heterozygous and wild-type mice were fed a normal diet (CMF; Oriental Yeast, Tokyo, Japan) as a negative control (intact group) (S-Table 1). Mice were sacrificed at 20 or 40 weeks of age. Animals in the AL treatment groups were subcutaneously injected with one dose of 20 μ l AL solution (60 mg/ml; dissolved in saline) 3 days postpartum.

Preliminary AL dose-finding study

We conducted the preliminary dose-finding study and administered seven doses of AL (at a maximum dose of 300 mg/ml) to the pups (S-Table 2). Pups died within 1 week following administration of AL doses of 80 mg/ml or higher. Thus, in the present study, an AL dose of 60 mg/ml was selected, which could allow pups to survive and not induce hyperglycemia. The mother animals were fed a normal diet (CMF) and allowed ad libitum access to tap water.

Glucosuria and glycemia monitoring

Urinary and blood glucose levels were measured every 5 weeks. Urinary glucose levels were measured semi-quantitatively using a urine test paper (Wako Pure Chemical Industries, Osaka, Japan). Blood glucose levels were measured semi-quantitatively using the glucose oxidase method (Glutest E; Sanwakagaku, Nagoya, Japan).

Oral glucose tolerance test, hematological analysis, and total carnitine assay

An oral glucose tolerance test (OGTT) was performed every 10 weeks until necropsy. After a 6 h fasting period, a 20% glucose solution (Otsuka Pharmaceutical Co., Ltd., Tokyo, Japan) was orally administered at a volume of 0.01 ml/g body weight per mouse; blood glucose levels were also measured immediately before administration and 15, 30, 60, and 120 min after administration. Serum insulin levels were measured using a murine enzyme-linked immunosorbent assay kit (Morinaga Institute of Biological Science, Inc., Kanazawa, Japan). As an alternative method for the assessment of IR, the homeostatic model assessment of IR (HOMA-IR) was calculated using the following formula: [fasting glucose (mmol/l) \times fasting insulin (ng/ml)]/22.4.

Aspartate aminotransferase (AST), alanine aminotransferase (ALT), triglyceride (TG), total cholesterol (T-CHO), high-density lipoprotein cholesterol (HDL-C), and low-density lipoprotein cholesterol (LDL-C) levels were measured by enzymatic methods using serum collected after necropsy.

Serum collected from male mice in the HF wild, HF hetero, and AL + HF wild groups at 40 weeks of age was also assayed for total carnitine using the enzymatic cycling method (Total carnitine "Kainos", Kainos Laboratories, Inc., Tokyo, Japan).

Histopathological analysis

The animals were euthanized after approximately 16 h of fasting. Blood samples were collected from the abdominal vena cava. The liver was excised, macroscopically examined, and weighed. The liver was then immersed in a 10% phosphate-buffered formalin solution. Formalin-fixed organs were trimmed, dehydrated, and embedded in paraffin wax. Sections (4- μ m thick) were stained with hematoxylin-eosin and Sirius red. All lesions were evaluated for the degrees of steatosis, lobular inflammation, and fibrosis according to Kleiner et al.²³. The ratio of fibrotic areas was determined using Sirius red-stained sections and image analysis software (IP Lab version 4.0; BD Biosciences, Rockville, MD, USA).

Immunohistochemical analysis

Immunohistochemical analysis was performed to identify the proliferative index (Ki-67), inflammatory cells (CD3, B220, Iba-1, and myeloperoxidase), and ductular reaction (cytokeratin [CK] 19) using representative sections of male mice at 20 and 40 weeks of age. Details regarding the primary antibody, antigen retrieval method, and secondary antibody are presented in S-Table 3²⁴. The Ki-67 positivity index of hepatocytes was calculated as the percentage of Ki-67-labeled nuclei/1000 hepatocytes. The positive areas of inflammatory cells and CK 19 were determined using image analysis software (IP Lab version 4.0; BD Biosciences).

Real-time polymerase chain reaction (PCR)

Gene expression involved in inflammation or fibrosis was analyzed using real-time PCR using fatty liver, fatty liver with rough surface (fibrosis), and fatty liver with nodule samples from 40-week-old male mice. Total RNA was extracted using the PureLink RNA Mini Kit (Life Technologies, Carlsbad, CA, USA). RNA was reverse-transcribed into cDNA using the High-Capacity RNA-to-cDNA Kit (Life Technologies). The cDNA was then subjected to quantitative real-time PCR (100 ng per reaction) and amplified with TaqMan Universal PCR Master Mix (Life Technologies) using the 7300 Real-Time PCR System (Life Technologies) with predeveloped TaqMan probe/primer combinations optimized by the manufacturer for interleukins (IL-1 β , IL-6), tumor necrosis factor alpha (TNF- α), transforming growth factor beta, organic cation/carnitine transporter 2, and superoxide dismutase 2. Threshold cycle numbers were transformed using the cycle threshold and relative value method described by the manufacturer and were expressed relative to glyceraldehyde-3-phosphate dehydrogenase, which was used as a housekeeping gene.

Statistical analysis

The results are expressed as the mean \pm standard deviation. A multiple comparison test was performed to analyze the differences between the

three or four groups. Homogeneity of variance was analyzed using Bartlett's test, followed by a one-way analysis of variance once the homogeneity of the variance was confirmed. If a significant difference was observed among the groups, Tukey's test was performed to compare the differences among the mean values. When the variance was heterogeneous, the Kruskal–Wallis H-test was performed. If a significant difference was observed among the groups, the nonparametric

Steel–Dwass test was used to compare the differences among the mean values. The difference was considered statistically significant with a calculated p -value < 0.05 . Statistical analyses were performed using the JMP Pro 13 software (SAS Institute Japan, Tokyo, Japan). All measured values of the inspection items obtained from heterozygous and wild-type mice fed a normal diet were within the normal range, and no significant difference was observed between the two groups in either sex. Thus, these data were grouped as an intact group and subjected to statistical processing.

RESULTS

HFD feeding induces obesity

All HFD-fed mice became obese, with a significant increase in their mean body weight with age in all HFD-fed groups compared with the intact group. There was no clear difference among the male mice in the HFD-treated groups, although the body weight of female mice in the AL + HF wild group was slightly lower than their respective counterparts in the other two HFD-treated groups after 15 weeks of age (Fig. 1A and S-Fig. 1).

Heterozygous mice show low serum carnitine levels

The serum carnitine levels in the male HF hetero group were significantly lower than in the male HF wild and male AL + HF wild groups at 40 weeks of age (Fig. 1B).

Neonatal AL treatment enhances IGT and IR

In the OGTT for males, blood glucose levels were higher in the HFD-fed groups than in the intact group at 20 weeks of age (Fig. 2). In particular, the AL + HF wild group showed a significantly higher value at up to 120 min at 20 weeks of age compared with the other two HFD-fed groups and the intact group. The increase in blood glucose levels in the AL + HF wild group at 40 weeks of age was milder than that observed at 20 weeks. In the OGTT for females, the blood glucose levels tended to increase in the AL + HF wild group compared with a milder increase in the blood glucose levels noted in males (S-Fig. 2). Additionally, fasting blood glucose levels tended to be higher in all HFD-treated male and female groups than in the intact group; however, the urinalysis results of almost all the mice did not detect glucose in urine.

In males, insulin levels and HOMA-IR scores were significantly higher at both 20 and 40 weeks of age in all HFD-fed groups than in the intact group. These values tended to decrease with age in

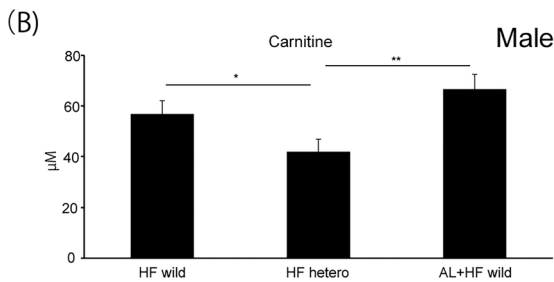
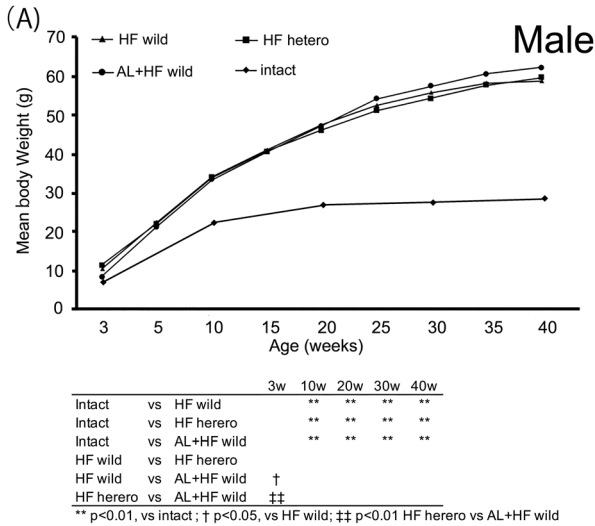


Fig. 1 The change in body weight in males and their total serum carnitine levels at 40 weeks of age. A Body weight. Data are expressed as the mean. **B** Serum total carnitine levels. Data are expressed as mean \pm standard deviation. * $p < 0.05$; ** $p < 0.01$.

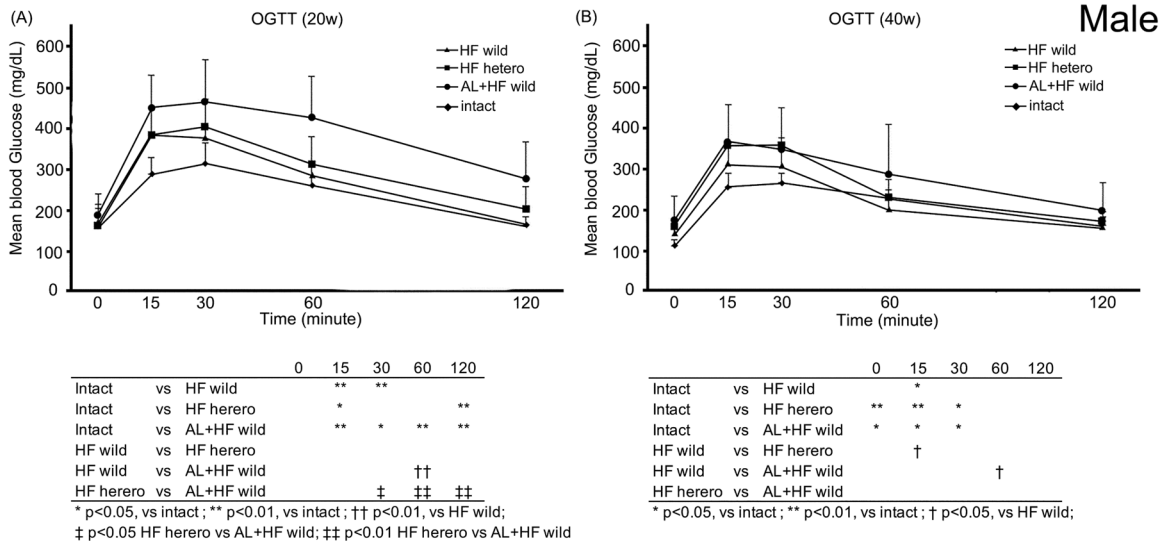


Fig. 2 The change in plasma glucose concentration during oral glucose tolerance test in males. A At 20 weeks of age. **B** At 40 weeks of age. Data are expressed as mean \pm standard deviation.

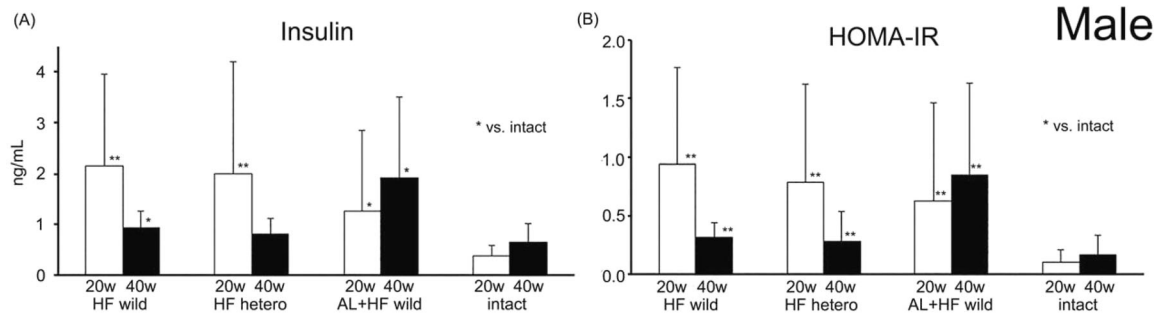


Fig. 3 Fasting insulin levels and, homeostatic model assessment of insulin resistance (HOMA-IR) score in male mice at 20 and 40 weeks of age. **A** Fasting serum insulin levels. **B** HOMA-IR score. Data are expressed as mean \pm standard deviation. * $p < 0.05$; ** $p < 0.01$.

the HF wild and HF hetero groups, although they tended to increase in the AL + HF wild group (Fig. 3). Females in all HFD-fed groups showed lower insulin levels and HOMA-IR scores compared with their male counterparts, and there was no clear difference among the HFD-fed groups (S-Fig. 3).

HFD feeding induces high AST, ALT, T-CHO, and LDL-C levels and increases liver weight

AST, ALT, T-CHO, and LDL-C levels increased with age in both sexes in all the HFD-treated groups; levels of these enzymes were significantly higher in HFD-treated mice at 40 weeks of age than in the intact group. Males showed higher values of these biochemical blood parameters compared with females. The mean values in the HFD-fed groups were comparable, and no increase in the mean values was observed between both sexes in the HF hetero and AL + HF wild groups compared with the HF wild group (Fig. 4 and S-Fig. 4).

HDL-C levels in all HFD-fed groups were almost the same as those in the intact group, regardless of sex. Additionally, TG levels were lower in all-male HFD-fed subjects at 20 and 40 weeks of age compared with their counterparts in the intact group, and there was no significant difference between the mean values observed in HFD-fed females and their counterparts in the intact group (Fig. 4 and S-Fig. 4).

The mean liver weight increased with age in both sexes in all HFD-treated groups, with subjects at 40 weeks of age exhibiting a significantly higher liver weight than those in the intact group. These values were also higher in males than in females (males, approximately 1.5 and 3 times more than that of the intact group at 20 and 40 weeks of age; females, about 1.2 and 2.4 times more than that of the intact group at the same age; Fig. 5A and B).

Low carnitine and early-stage induction of IGT enhance hepatocellular tumorigenesis

Macroscopically, fatty livers were observed in almost all HFD-fed mice of both sexes (Fig. 5C and F). Furthermore, fatty livers with rough surfaces corresponding to moderate to severe fibrosis were observed in each HFD-fed group in both the sexes, but the incidence did not increase with age in any HFD-fed group (Fig. 5D and F). Nodules developed in fatty livers with age in male HFD-fed mice, and the incidence rates in the HF hetero and AL + HF wild groups at 40 weeks of age (30% in each group) were remarkably higher than those in the HF wild group (7%) (Fig. 5E and F). Nodules were diagnosed as nodular hepatocellular hyperplasia or hepatocellular adenomas (Fig. 5G and H). The incidence rate of tumorigenesis in the male HF hetero and AL + HF wild groups was significantly increased with age (between 20 and 40 weeks of age) and reached 30% at 40 weeks of age in each group (Fig. 5H), but it was not significantly increased with age in the HF wild group, and the value was merely 7% at 40 weeks of age (Fig. 5H). To contrast, the incidence of fatty liver with nodules in female mice was

comparable in HFD-fed groups, and there was no clear difference among the HFD-treated groups (S-Fig. 5C).

HFD feeding induces NASH lesions similar to those induced by human NASH

In the hepatic centrilobular zone of almost all male HFD-treated mice, steatosis, and lobular inflammation were observed. These changes were accompanied by hepatocyte ballooning, degeneration, and regeneration and were noticeably enhanced in mice at 40 weeks of age compared with those at 20 weeks; however, there was no remarkable difference in the changes between the HFD-treated groups. Hepatic steatosis from the centrilobular to middle zone was observed in all the mice of the male AL + HF wild group and approximately 90% of the male HF wild and male HF hetero groups at 20 weeks of age (Fig. 6A). Severe hepatic steatosis regardless of lobules was noted in almost all 40-week-old male mice in the HFD-treated groups. Lobular inflammation was slightly observed in the male HFD-treated mice at 20 weeks of age, and the degree of inflammation progressed with age and was elevated at 40 weeks of age. The degree of inflammation in the HF hetero group at 40 weeks of age was significantly higher than in the AL + HF wild group; however, the degree of inflammation in these two groups did not significantly differ from that in the HF wild group (Fig. 6B). Hepatocellular ballooning was hardly observed at 20 weeks of age but was sporadically observed in approximately half of the male HFD-treated mice at 40 weeks of age (Fig. 6C). Even at 20 weeks of age, the degree of fibrosis in the HF hetero and AL + HF wild groups was significantly higher compared to the HF wild group. At 40 weeks of age, fibrosis was more evident along the sinusoids in the centrilobular zone (Fig. 6D), and there was no distinct difference in the degree of fibrosis between the HFD-treated groups. Fibrosis in non-cancerous tissue with nodules was more severe than in tissues without nodules (Fig. 6D). CK 19 and Ki-67-positive reactive bile ducts (ductal reaction) and oval cells were observed in the periportal to middle zone in all-male HFD-treated groups at 40 weeks of age (Fig. 7). Ki-67-positive cells were also observed in hepatocytes and were significantly increased in mice at 40 weeks of age compared with those at 20 weeks of age. Females had milder lesions compared with males, and there was no clear difference between the HFD-treated groups (S-Fig. 6).

CD3-positive T-cell infiltration and TNF- α mRNA level increase with NASH progression

Lobular inflammation consisted of neutrophils, a small number of T cells, B cells, and macrophages (Fig. 8A–D). In all the male HFD-treated groups, the number of neutrophils, T cells, and B cells was significantly increased or tended to increase in mice at 40 weeks of age compared with those at 20 weeks of age. Macrophages frequently aggregated and surrounded hepatocytes containing large lipid droplets in all-male HFD-treated groups at 40 weeks of

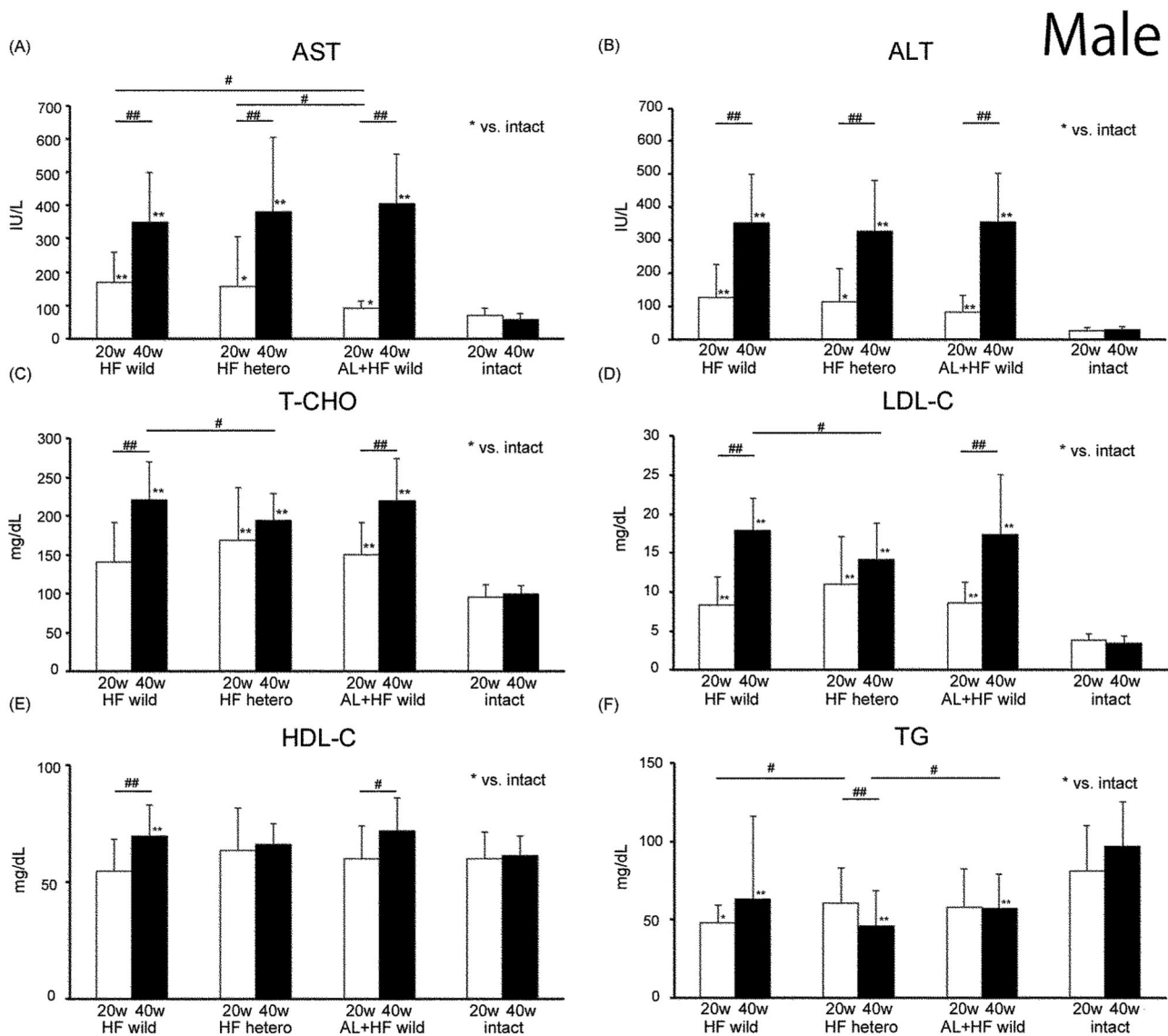


Fig. 4 Liver enzymes and cholesterol are increased in high-fat diet treatment in males. A Aspartate aminotransferase. **B** Alanine aminotransferase. **C** Total cholesterol. **D** Low-density lipoprotein cholesterol. **E** High-density lipoprotein cholesterol. **F** Triglycerides. Data are expressed as mean \pm standard deviation. * or # $p < 0.05$; ** or ## $p < 0.01$.

age, and macrophage infiltration was observed to increase with age in the male AL + HF wild group (Fig. 8D).

Upon comparison of inflammatory cytokine mRNA levels between fatty liver, fatty liver with rough surface (fibrosis), and fatty liver with nodules, a significant increase in mRNA levels of TNF- α was observed when fatty liver progressed and exhibited nodule formation (Fig. 8E). The mRNA levels of IL-6 also tended to increase as the lesion progressed (Fig. 8E). The mRNA expression of transforming growth factor beta was also remarkably increased in fatty livers with fibrosis compared to those without. Moreover, fatty livers with nodules showed a significantly higher number of CD-3-positive T cells than fatty livers without a rough surface (Fig. 8F).

DISCUSSION

We established two murine models for NASH in which the development of obesity, IGT, IR, high cholesterol, fatty liver, steatohepatitis, fibrosis, and eventually tumorigenesis was observed. Most conventional HFD-induced NASH models show

almost the same clinical and histopathological conditions as described above; however, tumor incidence is lower^{6-8,25} than in our two murine models. Among the reported HFD-induced NASH models, STAM mice treated with streptozotocin and HFD developed early-stage hepatocellular carcinoma. However, streptozotocin is a genotoxic substance and has a significant effect on tumorigenesis. Furthermore, this model does not include the development of obesity⁹. Therefore, there is no HFD-induced NASH animal model that completely matches human NAFLD/NASH pathophysiologically or pathologically. In this study, male wild-type mice treated with AL and HFD developed obesity, IGT, IR, high insulin level, high cholesterol, and a fatty liver at 20 weeks of age. At 40 weeks of age, fatty liver, steatohepatitis, and perisinusoidal fibrosis progressed in this group, and nodular hepatocellular hyperplasia and hepatic adenoma were detected in approximately 30% of mice. HFD-treated male heterozygous *jvs/+* mice also exhibited NASH to a similar extent and severity, and the incidence of tumor formation was similar to what was observed in AL and HFD-treated male wild-type mice. Therefore, it is highly probable that these two types of murine models are useful for

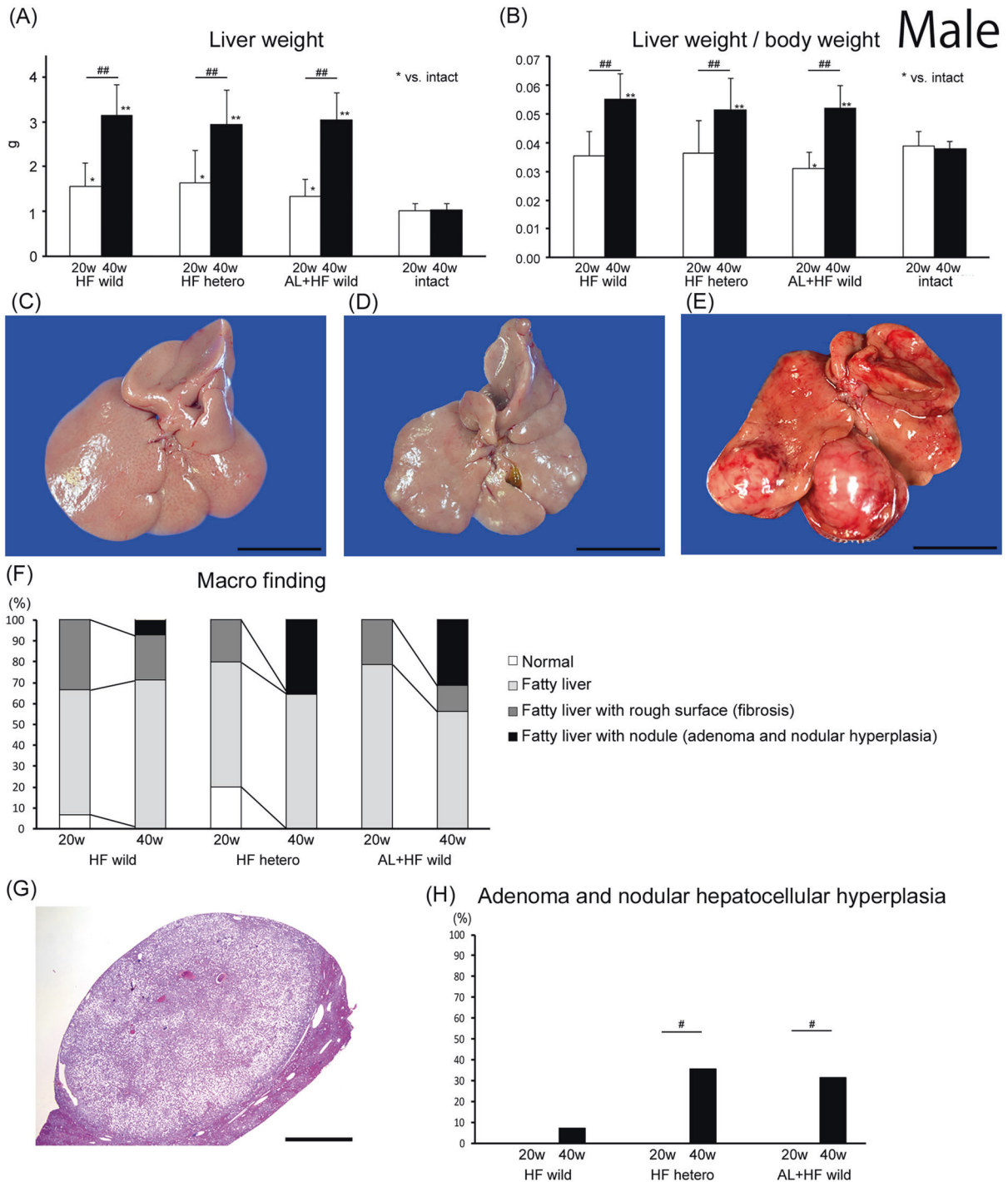


Fig. 5 Low carnitine and early-stage induction of impaired glucose tolerance enhance fatty liver and nodule formation in males. **A** Liver weight. **B** Liver-to-body weight. Data are expressed as mean \pm standard deviation. Representative macroscopic pictures of fatty liver **C**, fatty liver with rough surface (fibrosis) **D**, and steatosis with nodules (adenoma and hepatocellular hyperplasia) **E**. Scale bar is 10 mm. **F** Percentage of macroscopic findings. **G** Representative histological picture of hepatocellular adenoma (hematoxylin and eosin stain). Scale bar is 2 mm. **H** Percentage of hepatic adenoma and hepatocellular hyperplasia. Data are expressed as mean. * or #*p* < 0.05; ** or ##*p* < 0.01.

HFD-induced NASH models with proliferative lesions of hepatocytes, similar to that seen in human NASH.

Most human NAFLD/NASH patients have IR, high insulin levels, and IGT due to metabolic syndromes such as obesity and diabetes². In this study, AL- and HFD-treated male wild-type mice at 20 weeks of age clearly showed higher IGT by OGTT than the other two HFD-treated groups. AL reportedly destroys pancreatic β -cells and induces diabetes in experimental animals^{15,16}. In this

study, AL treatment for neonatal mice could not induce persistent diabetes but could induce transient IGT. Additionally, fasting blood glucose was slightly high, and no urinary glucose was detected in the neonates treated with AL. The high insulin level and HOMA-IR score suggest that β -cell hyperactivity and IR may occur at the neonatal stage in AL- + HFD-treated male mice. High HOMA-IR scores, high insulin levels, and IGT were also observed in the other two HFD-treated groups that had received no AL,

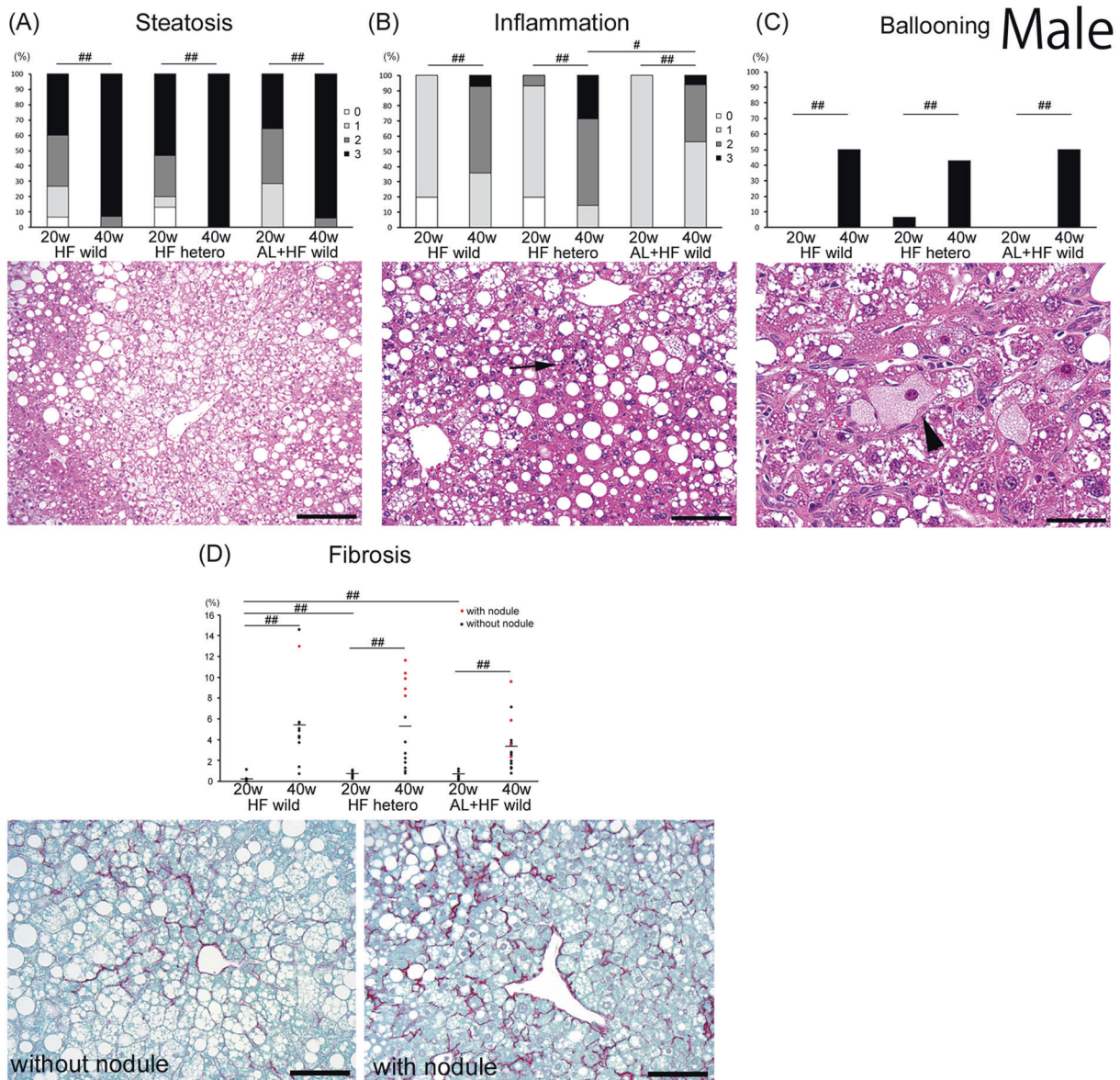


Fig. 6 High-fat diet (HFD) feeding induces nonalcoholic steatohepatitis lesions similar to human nonalcoholic steatohepatitis. Percentage of steatosis **A**, inflammation **B**, ballooning **C**, and fibrosis **D**. Representative hematoxylin and eosin-stained and Sirius red-stained images of male low-dose alloxan treatment HFD-fed wild groups at 40 weeks of age. Inflammation (**B**, arrow), ballooning (**C**, arrowhead), and collagen deposits (**D**, red staining). Hematoxylin and eosin (**A**, **B**, and **C**) and Sirius Red staining (**D**). Data are expressed as mean \pm standard deviation. Scale bars represent (**A**) 200 μ m, (**B**, **D**, and **E**) 100 μ m, and (**C**) 50 μ m. $^{\#}p < 0.05$; $^{\#\#}p < 0.01$.

consistent with the results of the HFD-induced obesity models in previous studies^{6,8,26}. However, only the AL and HFD-treated groups showed a time-course increase in insulin level and HOMA-IR score from 20 to 40 weeks of age, and the strongest IGT on OGTT among HFD-treated groups. These results suggest that AL administration in neonates further enhances IR and IGT compared with HFD treatment alone.

Male HFD-treated heterozygous *jvs/+* mice also showed more severe IGT and a higher incidence of tumor formation than male HFD-treated wild-type mice. Heterozygous *jvs/+* mice have lower carnitine levels in the plasma and liver than the wild-type mice and show a slight lipid accumulation in hepatocytes^{11–13}. The present study also confirmed that heterozygous *jvs/+* mice showed lower carnitine levels compared to the wild-type mice. Administration of L-carnitine to patients with NASH improves liver function, plasma glucose level, lipid profile, HOMA-IR score, and histopathological manifestations²⁷. Carnitine ameliorates fatty

liver and tumorigenesis in HFD-treated C57BL/6 STAM mice¹⁴. L-carnitine treatment also shows anti-tumor activity against hepatocellular carcinoma using cell lines and mouse models for hepatocellular carcinoma because of its histone deacetylase-inhibiting potential²⁸. Thus, low carnitine levels in heterozygous *jvs/+* mice may affect abnormal glucose metabolism and tumorigenesis.

The degree of liver fibrosis is the most reliable prognostic factor for NASH²⁹, and in this study, nodular lesions tended to develop in mice with severe fibrosis in the male HFD-fed groups. In addition, the degree of fibrosis with enhanced tumorigenesis was significantly higher in the HF hetero and AL + HF wild groups, even at 20 weeks of age, than in the HF wild group. These results suggest that liver fibrosis affects tumorigenesis in our model as well as in human NASH. The early expression of liver fibrosis at 20 weeks of age in the HF hetero and AL + HF wild groups was closely related to the low carnitine levels and early IGT expression induced by AL

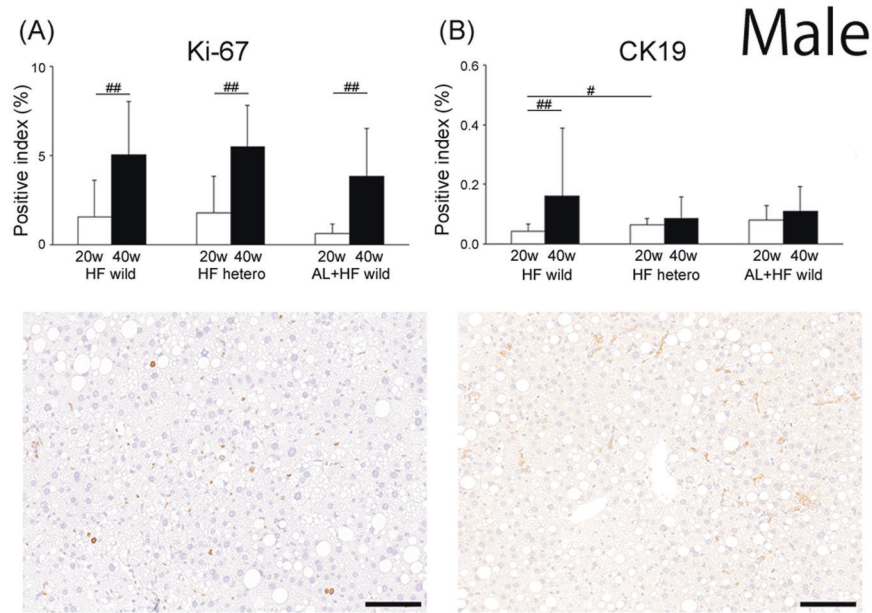


Fig. 7 High-fat diet (HFD) induces hepatocyte regeneration in males. Positive index of Ki-67 **A** and CK19 **B**, and each representative immunohistochemical stained images of male low-dose alloxan treatment HFD-fed wild groups at 40 weeks of age. Data are expressed as mean ± standard deviation. Scale bars are 100 µm. #*p* < 0.05; ##*p* < 0.01.

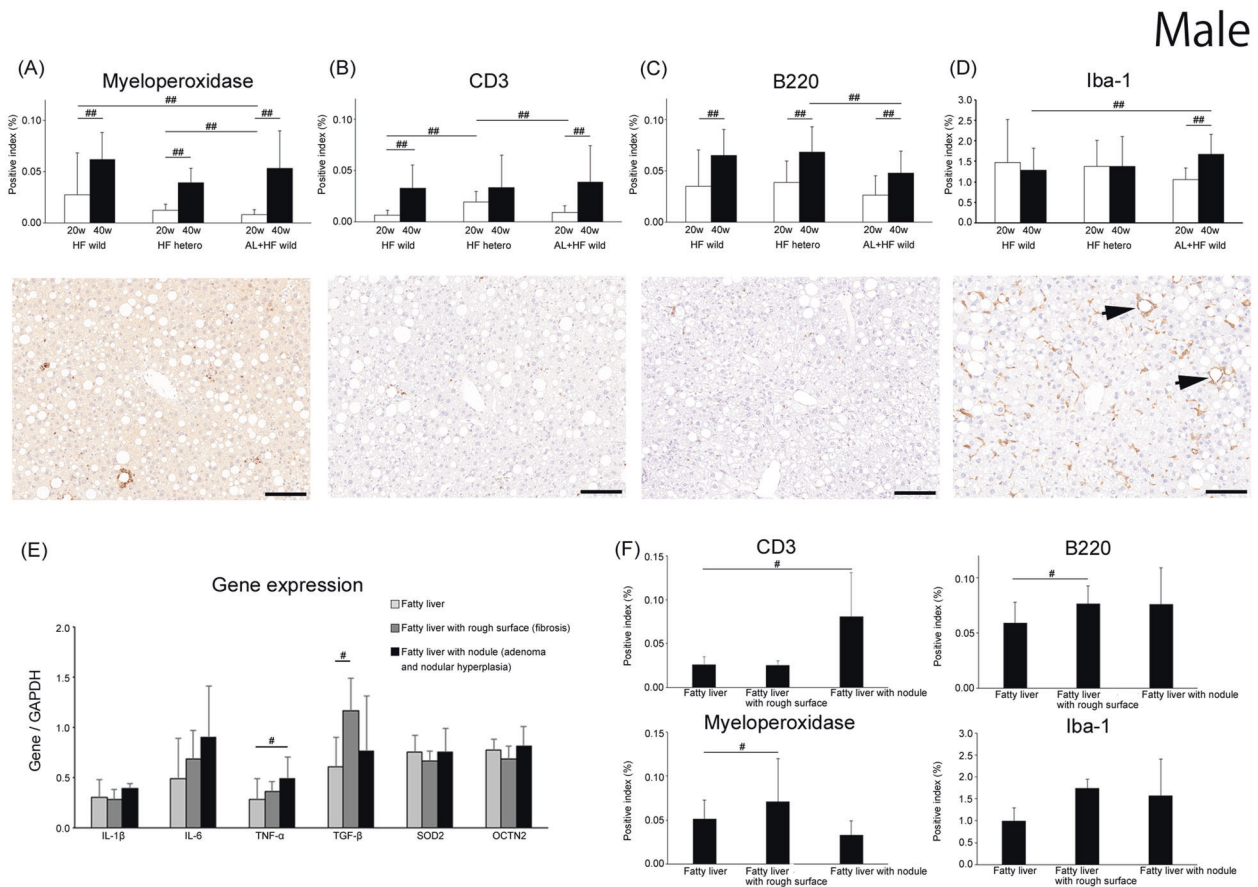


Fig. 8 CD3-positive T-cell infiltration and TNF-α mRNA level increase as nonalcoholic steatohepatitis progresses. Positive index of myeloperoxidase **(A)**, CD3 **(B)**, B220 **(C)**, and Iba-1 **(D)** and each representative immunohistochemical stained images of male low-dose alloxan treatment high fat diet-fed wild groups at 40 weeks of age. Iba-1-positive macrophages **(D)** frequently aggregate and surrounded hepatocytes containing large lipid droplets (arrows). In all pictures, the scale bar is 100 µm. **E** Hepatic gene expression for each lesion. **F** Positive index of CD3, B220, myeloperoxidase, and Iba-1 for each lesion in immunohistochemistry. Data are expressed as mean ± standard deviation. #*p* < 0.05; ##*p* < 0.01.

treatment, suggesting that this early development of liver fibrosis plays an important role in the enhanced tumorigenesis. In human NASH, the progression to hepatocellular carcinoma is usually mediated by fibrosis and cirrhosis throughout tumorigenesis; liver fibrosis progresses through varying stages to cirrhosis, which is a major risk factor for hepatocellular carcinoma²⁹. However, in our NASH model, fibrosis did not progress to the bridging stage or cirrhosis. Considering that hepatocellular carcinoma sometimes develops without cirrhosis involvement in human NASH^{30,31}, the tumorigenesis of our mouse models for NASH may be similar to that of human NASH without cirrhosis involvement.

Lobular inflammation comprising infiltration of neutrophils, lymphocytes, and macrophages was enhanced with the progression from fatty liver to nodule formation in HFD-treated male mice, similar to human NASH^{32,33}. The lobular inflammation in the HF hetero group was significantly increased compared with the AL + HF wild group. Carnitine supplementation reportedly has an anti-inflammatory effect both in humans and mice^{14,27}. Thus, the low carnitine levels in heterozygous *jvs/+* mice might have failed to suppress lobular inflammation caused by HFD treatment, resulting in a stronger lobular inflammation in the HF hetero group compared to the AL + HF wild group. However, the lobular inflammation level in the HF hetero group did not significantly differ from that in the HF wild group as a control, and there were no differences in AST and ALT values and hepatocyte ballooning among the three groups. Therefore, it is possible that the enhancement of hepatic inflammation in the HF hetero group might not be severe enough to exacerbate liver function and morphology. Further extension of the experimental period may clarify the pathological differences between the groups.

With the progression of lobular inflammation in these mice, the number of aggregated macrophages surrounding hepatocytes with large lipid droplets increased, which closely resembled the histopathological findings observed in human NASH and murine NASH models. This histological structure, termed as “hepatic crown-like structure”, may be involved in the development of inflammation in NASH^{34,35}. Macrophages produce TNF- α , IL-1, and IL-6 and promote the progression of NASH^{36–38}. In this study, TNF- α and IL-6 mRNA levels also increased as the liver disease progressed to fatty liver, fibrosis, and eventually to nodule formation. These findings suggest that lobular inflammation, including hepatic crown-like structure in our murine model, plays an important role in the progression of steatohepatitis, similar to human NASH.

Hepatocyte injury, including ballooning degeneration, develops along with exacerbation of inflammation in human NASH^{36–38}. Herein, we showed that the number of hepatocytes with ballooning degeneration was increased in HFD-treated male mice at 40 weeks of age compared with that at 20 weeks of age. Furthermore, in these mice, Ki-67-positive hepatocytes, CK19-positive ductular reaction, and oval cells were increased with enhanced degeneration, suggesting that hepatocyte regeneration also occurred. The ductular reaction increased along with fat accumulation and apoptosis in hepatocytes in human NASH^{39,40}. These results suggest that hepatocyte injury and regeneration in our murine model of NASH are also similar to the pathological conditions in human NASH.

We successfully established two novel mouse models for NASH that developed obesity, fatty liver, IR, fibrosis, and eventually tumorigenesis using male heterozygous *jvs/+* mice with low carnitine and male wild-type mice with IGT. These results suggest that low carnitine levels and early-stage induction of IGT are important factors in the progression of NASH to tumorigenesis, similar to observations in human NASH. Our models could be useful as experimental tools for the development of drugs and to clarify the pathogenesis of NASH.

Supplementary information is available at *Laboratory Investigation's* website.

DATA AVAILABILITY

The datasets used and/or analyzed during the current study are available from the corresponding author on reasonable request.

REFERENCES

- Sanches S. C., Ramalho L. N., Augusto M. J., da Silva D. M., Ramalho F. S. Non-alcoholic steatohepatitis: a search for factual animal models. *Biomed. Res. Int.* <https://doi.org/10.1155/2015/574832> (2015).
- Yu J., Marsh S., Hu J., Feng W., Wu C. The pathogenesis of nonalcoholic fatty liver disease: interplay between diet, gut microbiota, and genetic background. *Gastroenterol. Res. Pract.* <https://doi.org/10.1155/2016/2862173> (2016).
- Neuschwander-Tetri, B. A. Non-alcoholic fatty liver disease. *BMC Med.* **15**, 45 (2017).
- Day, C. P. & James, O. F. Steatohepatitis: a tale of two “hits”? *Gastroenterology* **114**, 842–845 (1998).
- Tilg, H. & Moschen, A. R. Evolution of inflammation in nonalcoholic fatty liver disease: the multiple parallel hits hypothesis. *Hepatology* **52**, 1836–1846 (2010).
- Fan, J. G. & Qiao, L. Commonly used animal models of non-alcoholic steatohepatitis. *Hepatobiliary Pancreat. Dis. Int.* **8**, 233–240 (2009).
- Hansen, H. H. et al. Mouse models of nonalcoholic steatohepatitis in preclinical drug development. *Drug Discov. Today* **22**, 1707–1718 (2017).
- Asgharpour, A. et al. A diet-induced animal model of non-alcoholic fatty liver disease and hepatocellular cancer. *J. Hepatol.* **65**, 579–588 (2016).
- Fujii, M. et al. A murine model for non-alcoholic steatohepatitis showing evidence of association between diabetes and hepatocellular carcinoma. *Med. Mol. Morphol.* **46**, 141–152 (2013).
- Nezu, J. et al. Primary systemic carnitine deficiency is caused by mutations in a gene encoding sodium ion-dependent carnitine transporter. *Nat. Genet.* **21**, 91–94 (1999).
- Kaido, M. et al. Mitochondrial abnormalities in a murine model of primary carnitine deficiency. Systemic pathology and trial of replacement therapy. *Eur. Neurol.* **38**, 302–309 (1997).
- Takahashi, R. et al. Pressure overload-induced cardiomyopathy in heterozygous carrier mice of carnitine transporter gene mutation. *Hypertension* **50**, 497–502 (2007).
- Lahjouji, K., Elimrani, I., Wu, J., Mitchell, G. A. & Qureshi, I. A. A heterozygote phenotype is present in the *jvs/+* mutant mouse livers. *Mol. Genet. Metab.* **76**, 76–80 (2002).
- Ishikawa H. et al. L-carnitine prevents progression of non-alcoholic steatohepatitis in a mouse model with upregulation of mitochondrial pathway. *PLoS One* <https://doi.org/10.1371/journal.pone.0100627> (2014).
- Reaven, G. M., Sageman, W. S. & Swenson, R. S. Development of insulin resistance in normal dogs following alloxan-induced insulin deficiency. *Diabetologia* **13**, 459–462 (1977).
- Ighodaro, O. M., Adeosun, A. M. & Akinloye, O. A. Alloxan-induced diabetes, a common model for evaluating the glycemic-control potential of therapeutic compounds and plants extracts in experimental studies. *Medicina* **53**, 365–374 (2017).
- Lazarow, A. Spontaneous recovery from alloxan diabetes in the rat. *Diabetes* **1**, 363–372 (1952).
- Rerup, C. C. Drugs producing diabetes through damage of the insulin secreting cells. *Pharmacol. Rev.* **22**, 485–518 (1970).
- Jain, D. K. & Arya, R. K. Anomalies in alloxan-induced diabetic model: it is better to standardize it first. *Indian J. Pharmacol.* **43**, 91 (2011).
- Simon, M. M. et al. A comparative phenotypic and genomic analysis of C57BL/6J and C57BL/6N mouse strains. *Genome Biol.* **14**, R82 (2013).
- Koizumi, T., Nikaido, H., Hayakawa, J., Nonomura, A. & Yoneda, T. Infantile disease with microvesicular fatty infiltration of viscera spontaneously occurring in the C3H-H-2(0) strain of mouse with similarities to Reye's syndrome. *Lab. Anim.* **22**, 83–87 (1988).
- Nikaido, H., Horiuchi, M., Hashimoto, N., Saheki, T. & Hayakawa, J. Mapping of *jvs* (juvenile visceral steatosis) gene, which causes systemic carnitine deficiency in mice, on chromosome 11. *Mamm. Genome* **6**, 369–370 (1995).
- Kleiner, D. E. et al. Design and validation of a histological scoring system for nonalcoholic fatty liver disease. *Hepatology* **41**, 1313–1321 (2005).
- Moroki, T. et al. Databases for technical aspects of immunohistochemistry: 2021 update. *J. Toxicol. Pathol.* **34**, 161–180 (2021).
- Cong, W. N., Tao, R. Y., Tian, J. Y., Liu, G. T. & Ye, F. The establishment of a novel non-alcoholic steatohepatitis model accompanied with obesity and insulin resistance in mice. *Life Sci.* **82**, 983–990 (2008).
- Wang, C. Y. & Liao, J. K. A mouse model of diet-induced obesity and insulin resistance. *Methods Mol. Biol.* **821**, 421–433 (2012).

27. Malaguenera, M. et al. L-carnitine supplementation to diet: a new tool in treatment of nonalcoholic steatohepatitis—a randomized and controlled clinical trial. *Am. J. Gastroenterol.* **105**, 1338–1345 (2010).
28. Huang H. et al. L-carnitine is an endogenous HDAC inhibitor selectively inhibiting cancer cell growth in vivo and in vitro. *PLoS One* <https://doi.org/10.1371/journal.pone.0049062> (2012).
29. Hashimoto, E., Tokushige, K. & Ludwig, J. Diagnosis and classification of non-alcoholic fatty liver disease and non-alcoholic steatohepatitis: current concepts and remaining challenges. *Hepatol. Res.* **45**, 20–28 (2015).
30. Carr, R. M., Oranu, A. & Khungar, V. Nonalcoholic fatty liver disease: pathophysiology and management. *Gastroenterol. Clin. North Am.* **45**, 639–652 (2016).
31. Michelotti, G. A., Machado, M. V. & Diehl, A. M. NAFLD, NASH and liver cancer. *Nat. Rev. Gastroenterol. Hepatol.* **10**, 656–665 (2013).
32. Farrell, G. C., van Rooyen, D., Gan, L. & Chitturi, S. Nash is an inflammatory disorder: pathogenic, prognostic and therapeutic implications. *Gut Liver* **6**, 149–171 (2012).
33. Nati, M. et al. The role of immune cells in metabolism-related liver inflammation and development of non-alcoholic steatohepatitis (NASH). *Rev. Endocr. Metab. Disord.* **17**, 29–39 (2016).
34. Itoh M. et al. Hepatic crown-like structure: a unique histological feature in non-alcoholic steatohepatitis in mice and humans. *PLoS One* <https://doi.org/10.1371/journal.pone.0082163> (2013).
35. Itoh M. et al. CD11c+ resident macrophages drive hepatocyte death-triggered liver fibrosis in a murine model of nonalcoholic steatohepatitis. *JCI Insight* <https://doi.org/10.1172/jci.insight.92902> (2017).
36. Cha, J. Y., Kim, D. H. & Chun, K. H. The role of hepatic macrophages in non-alcoholic fatty liver disease and nonalcoholic steatohepatitis. *Lab. Anim. Res.* **34**, 133–139 (2018).
37. Tosello-Trampont, A. C., Landes, S. G., Nguyen, V., Novobrantseva, T. I. & Hahn, Y. S. Kupffer cells trigger nonalcoholic steatohepatitis development in diet-induced mouse model through tumor necrosis factor- α production. *J. Biol. Chem.* **287**, 40161–40172 (2012).
38. Ganz, M. et al. Progression of non-alcoholic steatosis to steatohepatitis and fibrosis parallels cumulative accumulation of danger signals that promote inflammation and liver tumors in a high fat-cholesterol-sugar diet model in mice. *J. Transl. Med.* **13**, 193 (2015).
39. Gadd, V. L. et al. The portal inflammatory infiltrate and ductular reaction in human nonalcoholic fatty liver disease. *Hepatology* **59**, 1393–1405 (2014).
40. Overi, D., Carpino, G., Franchitto, A., Onori, P. & Gaudio, E. Hepatocyte injury and hepatic stem cell niche in the progression of non-alcoholic steatohepatitis. *Cells* **9**, 590 (2020).

ACKNOWLEDGEMENTS

The authors thank the students Yuki Nakatani, Takashi Yamagiwa, Takeshi Morio, Shiori Yoshida, and Kazue Akira for providing technical assistance. We would like to thank Editage (www.editage.com) for English language editing.

AUTHOR CONTRIBUTIONS

Y.T., S.N., K.M., and K.O. performed the experiments and generated, analyzed, and interpreted the data. Y.T. and S.N. drafted the manuscript. Y.T. and K.O. performed statistical analysis. Y.T., S.N., M.T., and K.O. were involved in data interpretation and technical and material support. K.O. conceived the idea, designed experiments, assisted in data analyses, and was involved in the drafting and critical review of the manuscript. All authors critically revised the manuscript for important intellectual content.

FUNDING

The authors received no specific funding for this work.

COMPETING INTERESTS

The authors declare no competing interests.

ETHICAL APPROVAL

This study was approved by the Committee for Animal Experiments of Setsunan University.

ADDITIONAL INFORMATION

Supplementary information The online version contains supplementary material available at <https://doi.org/10.1038/s41374-022-00732-8>.

Correspondence and requests for materials should be addressed to Kiyokazu Ozaki.

Reprints and permission information is available at <http://www.nature.com/reprints>

Publisher's note Springer Nature remains neutral with regard to jurisdictional claims in published maps and institutional affiliations.